


# NLO QCD parton shower matching for $pp \rightarrow e^+ \nu_e \mu^- \bar{\nu}_\mu \gamma + X$

Ivan Rosario <sup>1,\*</sup> Francisco Campanario<sup>1,†</sup> and Simon Plätzer<sup>2,3,‡</sup>

<sup>1</sup>*Theory Division, IFIC, University of Valencia-CSIC, E-46980 Paterna, Valencia, Spain*

<sup>2</sup>*Institute of Physics, NAWI Graz, University of Graz, Universitätsplatz 5, A-8010 Graz, Austria*

<sup>3</sup>*Particle Physics, Faculty of Physics, University of Vienna, Boltzmannngasse 5, A-1090 Wien, Austria*

We present the implementation of a new interface in VBFNLO 3.0 supporting all di-boson and tri-boson processes with fully leptonic final states, enabling NLO+PS matched calculations. To demonstrate its capabilities, we study parton shower effects in the tri-boson production process  $pp \rightarrow e^+ \nu_e \mu^- \bar{\nu}_\mu \gamma + X$  using Herwig 7.3 with NLO QCD amplitudes from VBFNLO 3.0. We estimate uncertainties from scale variations and analyze the impact of generation-level cuts on parton shower events. This study showcases the new interface's potential and provides insights into the interplay between fixed-order calculations and parton shower effects in multi-boson production processes, crucial for precision measurements and BSM searches at the LHC and future colliders.

## I. INTRODUCTION

The Standard Model (SM) stands as our most comprehensive and precise framework for understanding particle physics. At its core, it is a Quantum Field Theory governed by the principle of local gauge invariance, which dictates the nature of particle interactions. The discovery of the Higgs boson in 2012 by the CMS [1] and ATLAS [2] collaborations at the Large Hadron Collider (LHC) completed the experimental verification of SM particle spectrum, resolving the long-standing challenge of reconciling gauge boson masses with local gauge invariance through the mechanism of spontaneous symmetry breaking.

After the discovery of the Higgs boson, the focus of particle physics has shifted to precision measurements of SM parameters and searches for physics beyond the SM (BSM). High-mass or weakly interacting particles may induce subtle effects on distributions and cross-sections at LHC energies, necessitating high precision in both experimental and theoretical approaches. Multi-boson production processes offer a promising avenue for probing these deviations. As the SM gauge principle fully determines electroweak boson couplings, these processes facilitate systematic studies of BSM effects through frameworks like Effective Field Theories (EFTs).

Accurate comparison between theoretical predictions and experimental data relies heavily on event generators. These tools combine perturbative matrix element calculations with parton showers and non-perturbative effects to compute observable quantities. In this context, understanding the effects of parton showers on next-to-leading order (NLO) quantum chromodynamics (QCD) calculations becomes crucial for precise predictions and uncertainty estimation.

In this work, we study the parton shower effects on NLO QCD matrix elements in the tri-boson produc-

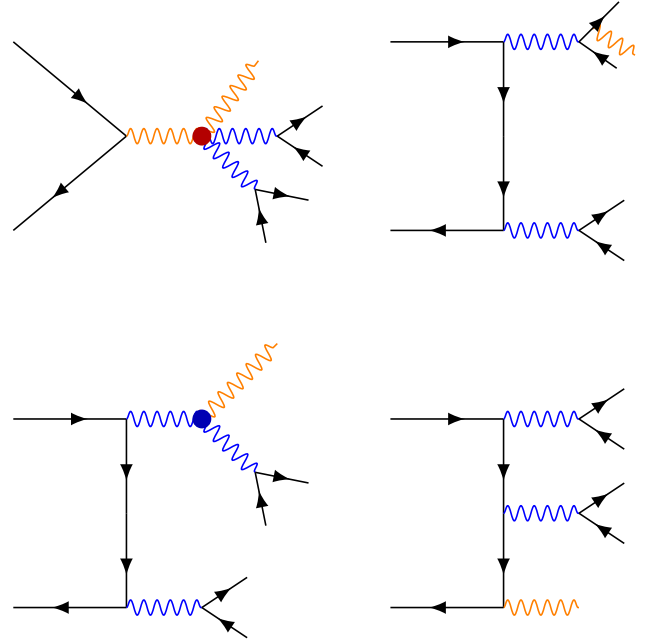


FIG. 1. Representative set of LO diagrams for tri-boson production processes. In the top left diagram, we can see a quartic gauge coupling (in red) where a s-channel photon decays into the two  $W$  and another photon. In the bottom left is a diagram with a triple gauge coupling (in blue), while the two right diagrams do not include any boson-boson coupling.

tion process  $pp \rightarrow e^+ \nu_e \mu^- \bar{\nu}_\mu \gamma (W^+ W^- \gamma)$  using the Herwig 7.3 event generator [3, 4] and VBFNLO 3.0 [5–8] as the NLO QCD amplitude provider. The communication between both programs is done through the BLHA interface. Tri-boson production processes have production cross-sections around the femtobarn. Despite this, several tri-boson production processes have been measured at the LHC by the ATLAS and CMS collaborations [9–12]. These processes are particularly interesting for BSM searches due to their sensitivity to anomalous gauge couplings and potential new physics in the electroweak sec-

\* ivan.rosario@ific.uv.es

† francisco.campanario@ific.uv.es

‡ simon.plaetzer@univie.ac.at

tor, see Fig. 1<sup>1</sup>. This analysis have been made possible by the recent implementation of the BLHA interface in VBFNLO 3.0, which is also available for the rest of the tri-boson and di-boson processes with fully leptonic final states.

We place particular emphasis on quantifying theoretical uncertainties from multiple sources. These uncertainties arise from two main factors: the truncation of the perturbative series in computing the hard collision matrix element, and the arbitrary cut-off scale in parton shower evolution that delineates the boundary between perturbative and non-perturbative scales. Understanding these uncertainties is crucial for interpreting experimental results and constraining BSM physics. We estimate them through variations of the factorization, renormalization, and hard shower scales.

Additionally, we study uncertainties related to shower-induced migration effects across kinematic cuts. The inclusion of generation-level cuts affects predictions at both the integrated and qS differential cross-section levels, as events that could potentially migrate into the accepted region after showering may be excluded at generation. This effect is particularly significant for safety cuts that are required for the simulation and influence QCD radiation, such as the Frixione Isolation cut. Furthermore, determining whether such cuts make predictions more or less inclusive requires dedicated analysis and cannot be assumed a priori. The resulting migration effects represent a source of uncertainty in the final prediction that must be carefully quantified.

This work is structured as follows: In Sec. II, we give the calculational setup, including programs, cuts, and other input parameters necessary to reproduce the results presented. In Sec. III, the differential distributions of different observables, with their corresponding scale variations at LO+PS, NLO and NLO+PS are presented and we study the migration effects of some generation level cuts. In Sec. IV, we present our conclusions.

## II. CALCULATIONAL SETUP

For this study, we use *Herwig* 7.3 as the Monte Carlo event generator and VBFNLO 3.0 as the NLO QCD amplitude provider. The communication between these programs is facilitated through the BLHA interface.

### A. NLO+PS Matching using *Herwig* 7.3

The *Herwig* 7.3 Monte Carlo event generator enables NLO event simulation through extensions to the previously developed Matchbox module [15], allowing external amplitude providers to evaluate tree-level and one-loop

matrix elements. These elements are automatically combined with the Catani-Seymour dipole subtraction [16], and general-purpose and specialized phase space generation algorithms, resulting in a full NLO calculation. This NLO calculation can be further extended by automatically determined matching subtractions, which combine it with a downstream parton shower algorithm.

While the Matchbox module supports a range of dedicated hard process calculations, communication with external general-purpose amplitude providers, such as VBFNLO 3.0, is facilitated through extensions to the BLHA 2 standard [17, 18].

### B. VBFNLO 3.0

VBFNLO 3.0 is a flexible Monte Carlo generator at the parton level for processes involving electroweak bosons. It is capable of providing a fully differential distributions at fixed-order parton level NLO QCD accuracy. Communication between VBFNLO 3.0 and *Herwig* 7.3 occurs via an interface built on the BLHA 2 standard [17, 18]. VBFNLO 3.0 has been extended to allow access to additional features such as the internal phase-space generator, which is used in the results presented in this article. However, these extensions are optional, and a Monte Carlo generator that complies with standard protocols is sufficient for obtaining amplitudes from VBFNLO 3.0.

The interface for Vector Boson Scattering of single and double vector boson production was previously performed and detailed results for the  $pp \rightarrow WWjj$  production channel were discussed in Ref. [19]. In this article, we extend the interface to all the double and triple boson production processes with fully leptonic decays and present detailed results for the process:

$$pp \rightarrow e^+ \nu_e \mu^- \bar{\nu}_\mu \gamma \quad (W^+ W^- \gamma) \quad (1)$$

The calculation is performed at order  $\alpha_s \alpha^2$  considering the massless fermion limit. The leptonic decay of the  $W$ -vectors are fully included, considering all off-shell effects and spin correlations. In Fig. 1, some representative graphs at LO showing the rich structure of the process can be found, including diagrams sensitive to quartic (top-left) and triple (bottom-left) gauge-boson vertices. It also shows examples of photons radiated off the leptons (top-right) or the quarkline (bottom-right) graphs which are considered to be irreducible backgrounds in the context of anomalous gauge coupling searches. The calculation of this process was presented first in Ref. [20] and release as part of the package VBFNLO 2.7[5]. We refer the reader to those references for details on the calculations and the test performed to cross-checked the calculation.

The accuracy of NLO fixed order predictions generated by the *Herwig* 7.3 + VBFNLO 3.0 through the BHLA 2 interface setup has undergone extensive validation against standalone calculations obtained from VBFNLO 3.0 predictions, using both a range of integrator and phase space

<sup>1</sup>The diagrams are made using FeynGame [13, 14]

generation algorithms supplied by the standard Matchbox modules or by utilizing the versatile interface structure to access the appropriate VBFNLO 3.0 routines.

### C. Matching algorithms and Uncertainties

The Matchbox module provides a wide range of options for generating matched cross sections via various algorithms, including direct and subtractive matching to both angular-ordered and dipole showers, as well as multiplicative (Powheg type) matching. Matchbox leverages adaptive methods to sample matrix-element corrections and adds, in case of angular-ordered showers, truncated showers to account for large-angle soft and hard collinear emissions on top of it.

To estimate theoretical uncertainties, we employ a combination of scale variations for the hard process and the parton shower. For the hard process, we use the 7-point variation scheme for the factorization ( $\mu_F$ ) and renormalization ( $\mu_R$ ) scales. This involves varying these scales independently by factors of 0.5 and 2 around the central scale, excluding the extreme variations (0.5, 2) and (2, 0.5). Independently, we vary the hard veto scale ( $\mu_Q$ ) of the shower by factors of 0.5 and 2. This approach results in a total of 9 variations: 7 from the hard process scale variations and 2 from the shower scale variations. We choose this method under the assumption that the shower and hard process variations are largely independent. A full combination of all scale variations would require significantly more computational resources. This approach provides a reasonable estimate of the uncertainties while remaining computationally feasible.

The `resummation` profile scale is used for both showers and the matrix-element correction entering the multiplicative matching to ensure a smooth transition between the hard matching and resummation regions, while maintaining the resummation properties of the parton shower.

### D. Cuts and phase-space optimization

In this subsection, we detail the parameters and settings used in our parton-level study of the process  $pp \rightarrow e^+ \nu_e \mu^- \bar{\nu}_\mu \gamma + X$  at  $\sqrt{s} = 13.6$  TeV.

#### 1. General Settings

We adopt a massless approximation for all partons and do not include multiple parton interactions (MPI). The Herwig 7.3 shower modules are used with their default settings.

#### 2. PDF and EW parameters

We use the CT18 PDF with four active flavours. The EW parameters are set to the standard values used in Herwig 7.3:

$$\begin{aligned} m_W &= 80.3770 \text{ GeV}, \quad \Gamma_W = 2.085 \text{ GeV} \\ m_Z &= 91.1876 \text{ GeV}, \quad \Gamma_Z = 2.495 \text{ GeV} \\ G_F &= 1.16637 \cdot 10^{-5} \text{ GeV}^{-2}. \end{aligned} \quad (2)$$

#### 3. Scale Choices

For both factorization and renormalization scales, we use the mass of the full EW system.

#### 4. Kinematic Cuts and Phase Space Optimization

We implement two sets of cuts: generation-level and analysis-level. Our default generation-level cuts, which we call “inclusive phase-space”, are:

$$\begin{aligned} p_{T,\ell} &> 10 \text{ GeV}, \quad |\eta_\ell| < 5.0 \\ p_{T,\gamma} &> 10 \text{ GeV}, \quad |\eta_\gamma| < 5.0, \\ \Delta R_{\ell\gamma} &> 0.3, \end{aligned} \quad (3)$$

The analysis-level cuts are tighter:

$$\begin{aligned} p_{T,\ell} &> 30 \text{ GeV}, \quad |\eta_\ell| < 2.5 \\ p_{T,\gamma} &> 30 \text{ GeV}, \quad |\eta_\gamma| < 2.5, \\ \Delta R_{\ell\gamma} &> 0.7, \end{aligned} \quad (4)$$

For photon isolation, we use the Frixione algorithm with  $\delta = 0.4$ ,  $\epsilon = 0.05$ . Jets are defined using the anti-kt algorithms with  $R = 0.4$  and  $p_T > 20$  GeV.

The runs have been made using an pre-optimized phase-space grid, which we refer to as the “tight phase-space”, applying the following cuts:

$$\begin{aligned} p_{T,\ell} &> 25, \text{ GeV}, \quad |\eta_\ell| < 3.0 \\ p_{T,\gamma} &> 25, \text{ GeV}, \quad |\eta_\gamma| < 3.0, \\ \Delta R_{\ell\gamma} &> 0.5. \end{aligned} \quad (5)$$

The primary purpose of this optimization is to enhance event generation efficiency while preserving the physical integrity of the predictions. By setting optimization cuts slightly looser than the analysis cuts, we ensure adequate sampling of events near the analysis cut boundaries.

The grid optimization and phase-space integration is performed using the MONACO sampler, a customized implementation of the VEGAS algorithm. Importantly, even when specific kinematic cut values are set during the grid pre-optimization phase-space integration, the event generation still produces events outside these ranges, provided they satisfy the generation-level cuts. This behavior occurs because MONACO optimizes a rectangular grid that increases point density in regions with large

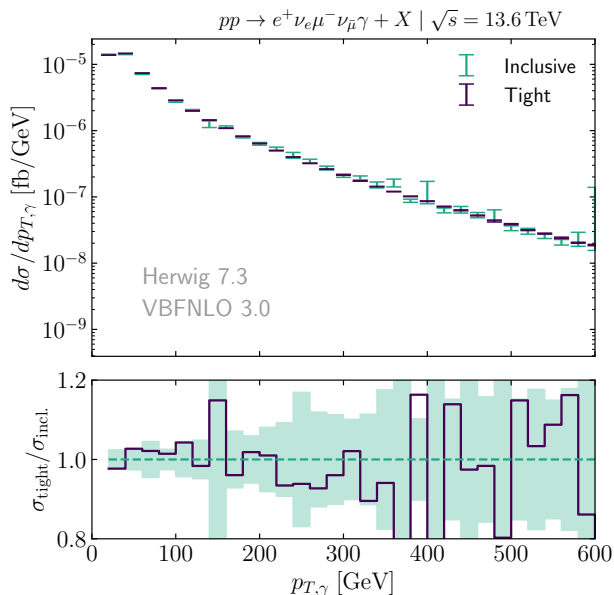


FIG. 2. Comparison between integrated cross-sections calculated using tight and inclusive phase space grids. Top panel: The differential cross-section  $d\sigma/dp_{T,\gamma}$  [fb/GeV] as a function of photon transverse momentum  $p_{T,\gamma}$  [GeV]. Purple curve shows results with tight phase space grid, blue curve shows inclusive phase space grid results, with statistical uncertainties indicated by error bars. Bottom panel: Ratio of tight to inclusive phase space cross-sections, with the shaded region representing the combined statistical uncertainty propagated from both calculations.

cross-sections, while still sampling points with wider grid spacing in regions with low cross-sections.

For clarity, the cuts in Eq. 5 are used solely to generate an optimized grid, improving the convergence of event generation. We maintain the cuts specified in Eq. 3 and Eq. 4 throughout all runs.

We have verified that this optimization introduces no artifacts by comparing differential distributions with lower-statistics runs using the generation level cuts to optimize the phase-space grid, Eq. 3. Fig. 2 demonstrates this comparison for the photon transverse momentum distribution. The excellent agreement between the tight and inclusive phase-space results confirms the validity of our approach, ensuring that our predictions remain physically meaningful while benefiting from improved computational efficiency.

### III. PHENOMENOLOGICAL RESULTS

In this section, we present and analyze the results of our parton shower matching study for the tri-boson production process  $pp \rightarrow e^+\nu_e\mu^-\bar{\nu}_\mu\gamma + X$  at  $\sqrt{s} = 13.6$  TeV. We focus on two key aspects: scale variations and migration effects.

Scale variations provide crucial insights into the the-

oretical uncertainties arising from the truncation of the perturbative series and the arbitrary separation between perturbative and non-perturbative regimes. By examining these variations, we can assess the reliability of our predictions and identify regions where higher-order corrections may be significant.

Migration effects, on the other hand, help us understand how parton shower emissions can shift event kinematics across cut boundaries, potentially impacting experimental analyses.

Our analysis encompasses fixed-order NLO results, LO+PS predictions, and NLO+PS simulations using both dipole and angular-ordered showers. By comparing these different approaches, we aim to elucidate the impact of parton showers on various observables and provide guidance for future experimental and theoretical studies of multi-boson production processes.

#### A. Scale variations

Fig. 3 presents a comprehensive analysis of the electroweak system's invariant mass distribution and its associated scale uncertainties. The main panel shows differential distributions calculated using various approaches: fixed-order NLO calculations (green), LO+PS predictions (pink), and NLO-matched results using both dipole (orange) and angular-ordered (blue) showers.

The uppermost ratio panel compares each prediction to the fixed-order NLO result, with the LO+PS ratio displayed on a separate scale (right axis) due to its larger variation. The four lower panels illustrate the cumulative impact of different scale variations on the differential cross-section. These panels use increasing opacity to show the sequential effects of varying the factorization ( $\mu_F$ ) and renormalization ( $\mu_R$ ) scales (darkest band), the hard veto scale ( $\mu_Q$ ), and finally, the total combined uncertainty ( $\mu_T$ , lightest band). All scale variations follow the scheme detailed in Sec. II C.

The invariant mass distribution of the EW-system is minimally affected by parton showering at NLO, and both, the angular-ordered and dipole showers, produce similar predictions for the central values and scale variations. The uncertainty in the scale variation is dominated by the renormalization and factorization scales in this observable, with a total scale variation of  $\pm 5\%$ . Notably, the LO+PS central value fails to predict the NLO result both in shape and normalization. This discrepancy arises from substantial NLO contributions, due to the colorless nature of the LO production process final state, including significant new contributions from gluon-initiated processes and the emergence of new phase-space regions. These effects manifest as a hard jet recoiling against the electroweak system, highlighting the importance of full NLO-matched results.

In contrast, jet observables are markedly influenced by parton shower effects, as illustrated in Fig. 4, which shows the differential distribution of the leading jet's

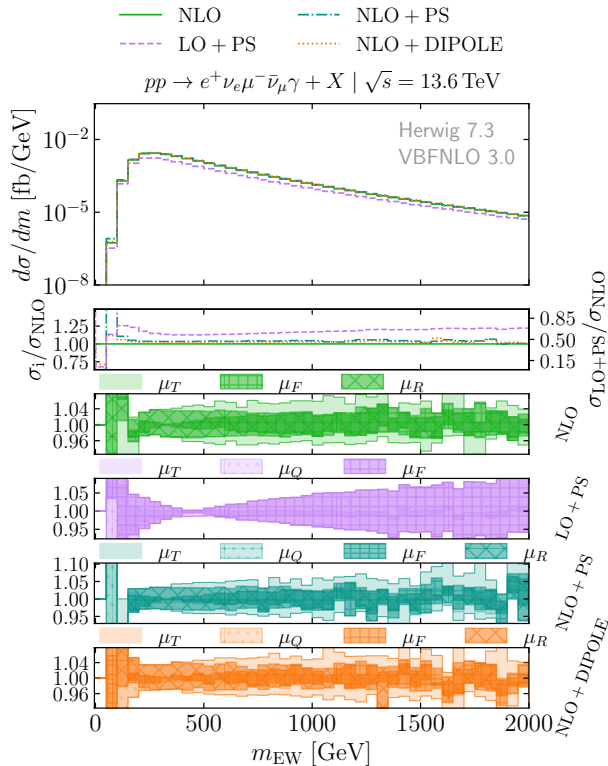


FIG. 3. Distribution of the electroweak system invariant mass showing fixed-order NLO (green), LO+PS (pink), and NLO matched predictions with angular-ordered (blue) and dipole (orange) showers. Top ratio panel compares all predictions to the NLO fixed-order result, with the LO+PS ratio shown on a separate scale (right axis). Lower panels display scale variation bands for each prediction type, with increasing opacity indicating the cumulative effect of different scale variations: factorization and renormalization scales (darkest), hard veto scale, and total combined uncertainty (lightest).

transverse momentum. At LO+PS, the jet consists solely of parton shower radiation, while in the NLO matched simulation, it is present at the matrix element level. Consequently, we anticipate larger uncertainties and a more pronounced impact of showering. In the NLO+PS scenario, the jet's transverse momentum distribution remains relatively stable with respect to shower effects at low to moderate  $p_T$ , typically within 10 – 20% of the fixed-order prediction.

The scale variation uncertainties exhibit a particularly dramatic improvement when moving from LO+PS to NLO+PS predictions. At LO+PS, variations are dominated by the hard veto scale, reaching up to 70% in the tail of the distribution. The inclusion of real radiation at NLO substantially reduces these uncertainties, resulting in more moderate variations ranging from a few percent at low  $p_T$  to approximately  $\pm 20\%$  at  $p_{T,j} = 800$  GeV.

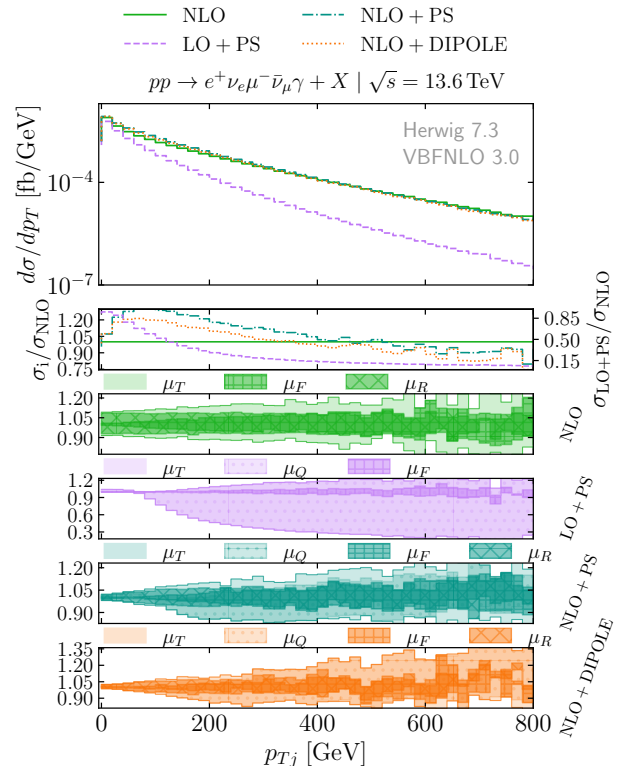


FIG. 4. Distribution of the leading jet transverse momentum showing fixed-order NLO (green), LO+PS (pink), and NLO matched predictions with angular-ordered (blue) and dipole (orange) showers. Top ratio panel compares all predictions to the NLO fixed-order result, with the LO+PS ratio shown on a separate scale (right axis). Lower panels display scale variation bands for each prediction type, with increasing opacity indicating the cumulative effect of different scale variations: factorization and renormalization scales (darkest), hard veto scale, and total combined uncertainty (lightest).

## B. Study of the migration effects

In this subsection, we examine the impact of migration through cut boundaries resulting from kinematical shifts induced by additional radiation in the parton shower. This phenomenon is crucial for understanding the interplay between theoretical calculations and experimental measurements.

Selection cuts in experimental analyses should ideally be applied at the event level after the parton shower process while keeping the fixed order prediction fully inclusive. However, this approach can significantly reduce computational efficiency, particularly for processes with highly exclusive cuts such as Vector Boson Scattering (VBS), since many generated events will be discarded by the analysis cuts.

In some cases, generation-level cuts cannot be avoided, such as when safety cuts are required to prevent theoretical divergences. Examples include the Frixione Isolation cut or minimum separation requirements between pho-

tons and charged leptons. Moreover, when events can have negative weights, the impact of these cuts becomes highly non-trivial – modifying cut parameters may either increase or decrease the total cross-section in ways that cannot be predicted without explicit calculation. This makes it impossible to determine a priori whether certain cut choices lead to more inclusive or exclusive selections.

In these cases, the effect of generation-level cuts must be incorporated as an additional theoretical uncertainty in the prediction. This uncertainty can often be estimated by varying the parameters of the generation-level cuts.

The effects of the parton shower in relation to cuts can be categorized into two distinct phenomena. Firstly, discrepancies between parton shower and fixed-order kinematics lead to variations in differential distributions due to analysis-level cuts. Secondly, the presence of generation-level cuts can induce migration effects, whereby shower-induced kinematic changes may allow events initially excluded by generation cuts to potentially fall within the analysis-permitted kinematic region.

We now focus on the migration effects as defined previously. Our analysis examines the impact of modifying the generation-level cuts for charged leptons and photon selection criteria. We present two types of results: the effect on the integrated cross-section and on differential distributions.

Fig. 5 illustrates the impact of varying the photon transverse momentum generation threshold on the integrated cross-section. The purple curve represents the parton shower result, while the blue curve shows the fixed-order calculation. As anticipated, the fixed-order calculation remains largely unaffected by the generation-level cut, with minor variations attributable to statistical fluctuations. This behavior is expected because fixed-order calculations do not include the additional radiation that can cause migration effects.

In contrast, the parton shower exhibits a more pronounced effect, with the integrated cross-section decreasing as the generation-level cut approaches the analysis cut. This trend can be understood as follows: as the generation-level cut approaches the analysis cut, there's less phase space for events to migrate into the analysis region due to shower effects, leading to a decrease in the accepted cross-section. This observation underscores the importance of careful consideration of generation-level cuts in shower-matched predictions, particularly for processes with tight kinematic selections.

To elucidate the impact on differential distributions, we refer to Fig. 6. This figure displays the differential distribution  $d\sigma/dp_{T,\gamma}$  as a function of the photon transverse momentum  $p_{T,\gamma}$ . The main plot features four curves corresponding to different values of the generation-level cut: 5 GeV, 10 GeV, 20 GeV, 30 GeV. The lower panel presents the ratio with respect to the lowest value of the transverse momentum generation-level cut (5 GeV), with the filled region indicating the missing cross-section.

Examining the figure reveals that the differential dis-

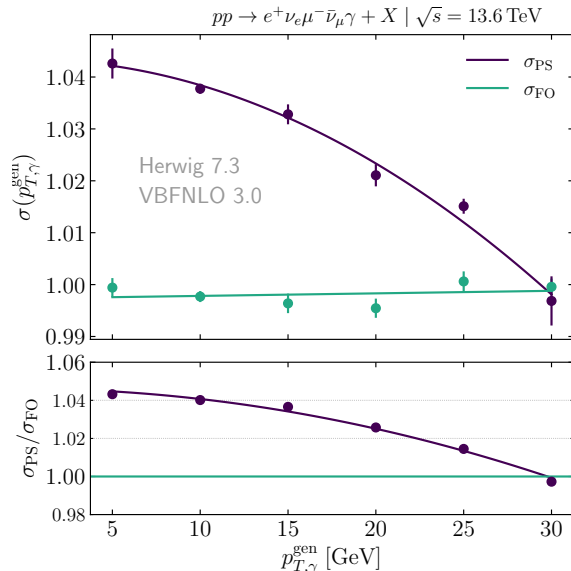


FIG. 5. Dependence of the integrated cross-section of the generation-level photon  $p_{T,\gamma}^{\text{gen}}$  cut. Top panel: integrated cross-section  $\sigma(p_{T,\gamma}^{\text{gen}})$  for parton shower (PS) and fixed-order (FO). Bottom panel: Ratio of the PS over FO cross-section.

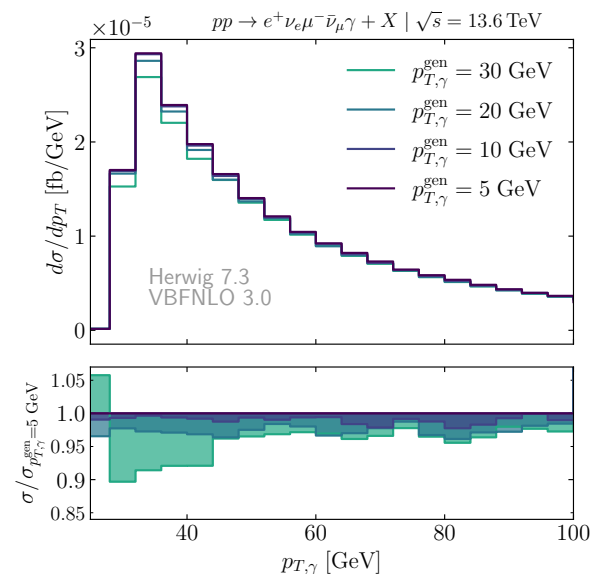


FIG. 6. Differential cross-section for the process  $pp \rightarrow e^+ \nu_e \mu^- \bar{\nu}_\mu \gamma + X$  at  $\sqrt{s} = 13.6$  TeV. Top panel: The differential cross-section  $d\sigma/dp_{T,\gamma}$  [fb/GeV] is shown as a function of the photon transverse momentum  $p_{T,\gamma}$  [GeV]. Four curves for different generation-level photon  $p_{T,\gamma}^{\text{gen}}$  cuts: 5 GeV, 10 GeV, 20 GeV, and 30 GeV. Bottom panel: Ratio of the cross-sections for different  $p_{T,\gamma}^{\text{gen}}$  generation cuts relative to the 5 GeV generation cut.



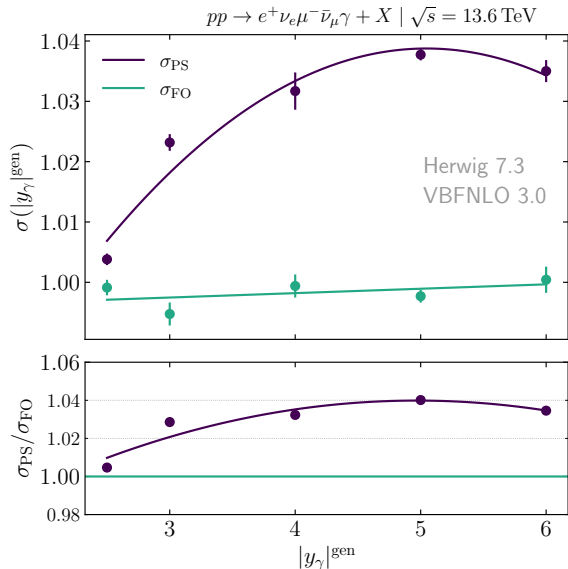


FIG. 7. Dependence of the integrated cross-section of the generation-level photon  $|y_\gamma|^{\text{gen}}$  cut. Top panel: integrated cross-section  $\sigma(|y_\gamma|^{\text{gen}})$  for parton shower (PS) and fixed-order (FO). Bottom panel: Ratio of the PS over FO cross-section.

tribution is not uniformly affected across all momentum ranges. The effects are more pronounced at lower transverse momenta, specifically for  $p_{T,\gamma} < 50$  GeV. This observation can be attributed to the proximity to the cut threshold, where smaller kinematic shifts induced by the shower are sufficient to exclude events from the analysis. As  $p_{T,\gamma}$  increases, the curves for different generation-level cuts converge, indicating that migration effects become less significant for high- $p_T$  photons, where the shower-induced kinematic shifts are relatively small compared to the photon's transverse momentum.

Fig. 7 presents the resulting integrated cross-sections as a function of the photon's rapidity generation-level cut,  $\sigma(|y_\gamma|^{\text{gen}})$ , where we observe patterns similar to those in the transverse momentum study. The fixed-order prediction (blue curve) maintains its expected insensitivity to the rapidity cut, while the parton-showered calculation (purple curve) exhibits a systematic decrease in cross-section as the rapidity cut becomes more restrictive (i.e., with decreasing  $|y_\gamma|^{\text{gen}}$ ). The corresponding differential distribution, shown in Fig. 8, reveals that the most pronounced effects occur near the cut boundary, with variations exceeding 10% at  $|y_\gamma|^{\text{gen}} = 3.0$ . Figs. 9-12 present analogous results for the positron, showing both the integrated cross-sections and differential distributions. These results mirror those observed for the photon and are included for completeness without further discussion.

Although our analysis uses more extreme generation-level cuts than those typically employed in experimental settings, we observe that these cuts can impact differ-

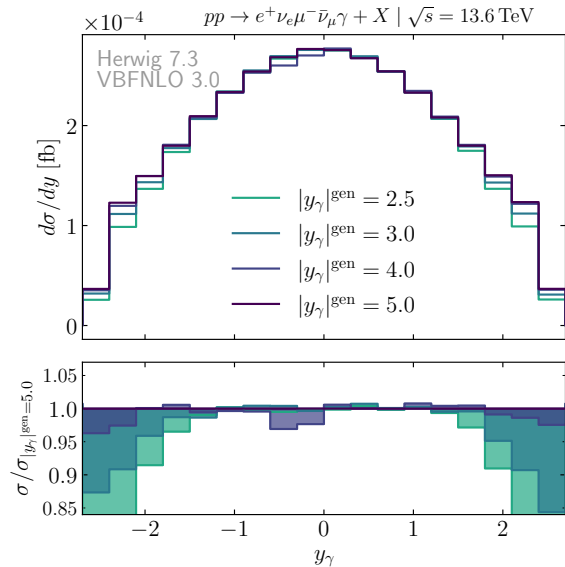


FIG. 8. Differential cross-section for the process  $pp \rightarrow e^+ \nu_e \mu^- \bar{\nu}_\mu \gamma + X$  at  $\sqrt{s} = 13.6$  TeV. Top panel: The differential cross-section  $d\sigma/dy_\gamma$  [fb] is shown as a function of the photon rapidity  $y_\gamma$ . Four curves for different generation-level photon  $y$  cuts ( $|y_\gamma|^{\text{gen}}$ ): 2.5, 3.0, 4.0 and 5.0. Bottom panel: Ratio of the cross-sections for different  $|y_\gamma|^{\text{gen}}$  generation cuts relative to the 5.0 generation cut.

ential distributions by up to 10%. This effect becomes particularly significant when compared to scale variation uncertainties of approximately  $\pm 5\%$ . The implications are especially relevant for analyses using highly inclusive cuts or processes requiring stringent kinematic constraints, such as Vector Boson Scattering (VBS). Furthermore, certain cuts like the Frixione Isolation cannot be removed, and estimating the parton shower effect and their associated uncertainties due to this cut is non-trivial. A more comprehensive treatment of such cases would require the inclusion of fragmentation functions to eliminate the need for these cuts altogether.

These findings underscore the critical interplay between parton shower effects and kinematic cuts, highlighting the necessity for careful consideration of generation-level constraints in precision phenomenological studies of multi-boson production processes. This is particularly important for ensuring reliable theoretical predictions that can be meaningfully compared with experimental measurements.

#### IV. CONCLUSIONS

VBFNLO 3.0 now incorporates BLHA interface support for all di-boson and tri-boson processes with fully leptonic final states, substantially enhancing our capabilities to study multi-boson production processes. This imple-

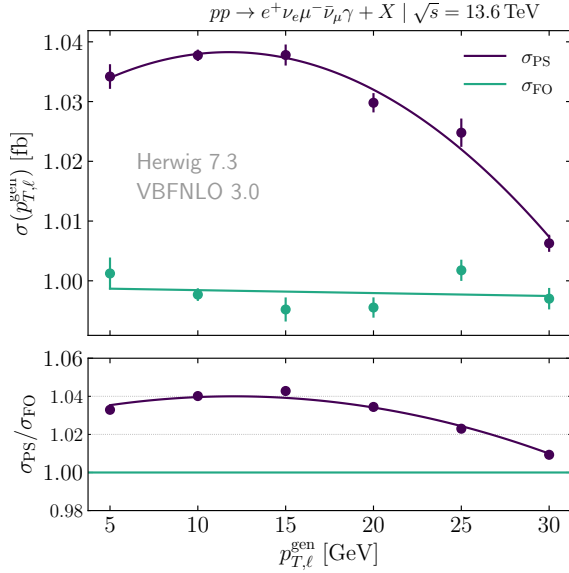


FIG. 9. Dependence of the integrated cross-section of the generation-level charged lepton  $p_{T,\ell}^{\text{gen}}$  cut. Top panel: integrated cross-section  $\sigma(p_{T,\ell}^{\text{gen}})$  for parton shower (PS) and fixed-order (FO). Bottom panel: Ratio of the PS over FO cross-section.

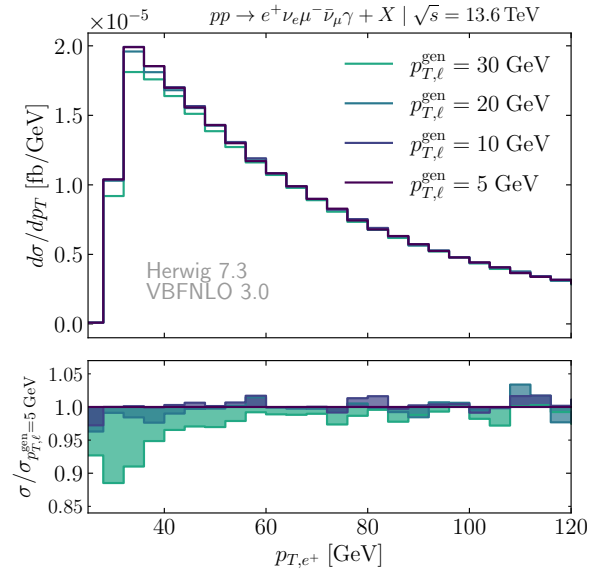


FIG. 10. Differential cross-section for the process  $pp \rightarrow e^+ \nu_e \mu^- \bar{\nu}_\mu \gamma + X$  at  $\sqrt{s} = 13.6$  TeV. Top panel: The differential cross-section  $d\sigma/dp_{T,e^+}$  [fb/GeV] is shown as a function of the positron transverse momentum  $p_{T,e^+}$  [GeV]. Four curves for different generation-level charged lepton  $p_{T,\ell}^{\text{gen}}$  cuts: 5 GeV, 10 GeV, 20 GeV, and 30 GeV. Bottom panel: Ratio of the cross-sections for different  $p_{T,\ell}^{\text{gen}}$  generation cuts relative to the 5 GeV generation cuts.

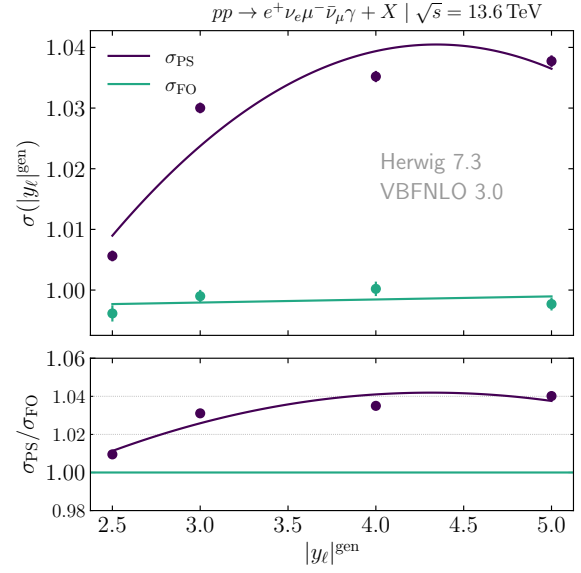


FIG. 11. Dependence of the integrated cross-section of the generation-level charged lepton  $|y_\ell|^{\text{gen}}$  cut. Top panel: integrated cross-section  $\sigma(|y_\ell|^{\text{gen}})$  for parton shower (PS) and fixed-order (FO). Bottom panel: Ratio of the PS over FO cross-section.

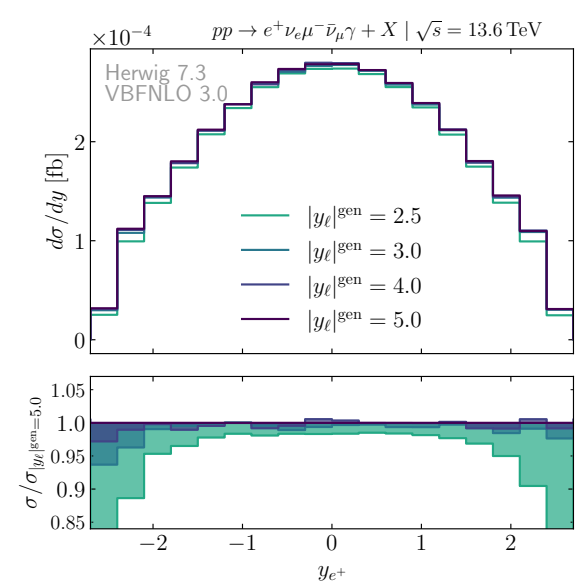


FIG. 12. Differential cross-section for the process  $pp \rightarrow e^+ \nu_e \mu^- \bar{\nu}_\mu \gamma + X$  at  $\sqrt{s} = 13.6$  TeV. Top panel: The differential cross-section  $d\sigma/dp_{T,e^+}$  [fb/GeV] is shown as a function of the positron rapidity  $y_{e^+}$  [GeV]. Four curves for different generation-level charged lepton  $|y_\ell|^{\text{gen}}$  cuts: 2.5, 3.0, 4.0 and 5.0. Bottom panel: Ratio of the cross-sections for different  $|y_\ell|^{\text{gen}}$  generation cuts relative to the 5.0 generation cut.



mentation enables NLO+PS matched calculations across a wide range of multi-boson channels, facilitating precise predictions that combine the accuracy of fixed-order calculations with the detailed final-state modeling of parton showers.

Our comprehensive analysis of the tri-boson production process  $pp \rightarrow e^+ \nu_e \mu^- \bar{\nu}_\mu \gamma + X$  at  $\sqrt{s} = 13.6$  TeV reveals several key insights into the interplay between NLO QCD calculations and parton shower effects. The study of scale variations demonstrates that electroweak system observables, such as the invariant mass, remain relatively stable under showering, with uncertainties dominated by renormalization and factorization scale variations (approximately  $\pm 5\%$ ). In contrast, jet observables show more pronounced shower effects and exhibit a dramatic reduction in uncertainties when moving from LO+PS to NLO+PS predictions, particularly in the high- $p_T$  regime where variations decrease from  $\approx 70\%$  to  $\approx 20\%$ .

The investigation of migration effects has revealed significant implications for experimental analyses and theoretical predictions. Our detailed study of generation-level cuts for photon and lepton kinematics demonstrates that parton shower effects can lead to substantial migrations across cut boundaries, with impacts of up to 10% on differential distributions - comparable to or exceeding the scale variation uncertainties. These effects are particularly pronounced near kinematic thresholds and become more significant with tighter rapidity cuts. The observed migration patterns differ markedly between fixed-order and showered predictions, with the latter showing systematic dependence on the generation-level cuts that must be carefully considered in precision studies.

Our findings demonstrate that NLO+PS matched calculations are essential for precise predictions in multi-boson production processes, especially when studying observables sensitive to jet activity. Generation-level cuts must be chosen carefully, as they can substantially influ-

ence final distributions even after applying analysis-level cuts. The observation that migration effects can match or exceed scale variation uncertainties indicates these effects warrant systematic inclusion in uncertainty estimates.

The expanded capabilities of VBFNLO 3.0 through the BLHA interface open new avenues for investigation in multi-boson physics. Future studies could extend this analysis to other channels, investigate the impact on searches for anomalous gauge couplings, and compare results across different event generators and parton shower algorithms. Such comparisons would be particularly valuable for establishing the robustness of predictions in regions where migration effects are significant.

## V. DISCLAIMER

The authors acknowledge the use of generative AI, specifically Claude 3.5 Sonnet, in the preparation of this manuscript. This AI tool was employed to enhance the flow, clarity, and grammatical quality of the text. While the scientific content, analysis, and conclusions remain the sole work of the human authors, the AI assistance has contributed to improving the overall readability and coherence of the paper. The authors have carefully reviewed and verified all AI-generated content to ensure its accuracy and alignment with the intended scientific message.

## VI. ACKNOWLEDGMENTS

F.C. and I.R. acknowledge financial support by the Generalitat Valenciana, the Spanish government and ERDF funds from the European Commission (Grants No. SEJI-2017/2017/019, CNS2022-136165, PID2023-151418NB-I00).

- 
- [1] Serguei Chatrchyan et al. Observation of a New Boson at a Mass of 125 GeV with the CMS Experiment at the LHC. *Phys. Lett. B*, 716:30–61, 2012.
  - [2] Georges Aad et al. Observation of a new particle in the search for the Standard Model Higgs boson with the ATLAS detector at the LHC. *Phys. Lett. B*, 716:1–29, 2012.
  - [3] M. Bahr et al. Herwig++ Physics and Manual. *Eur. Phys. J. C*, 58:639–707, 2008.
  - [4] Johannes Bellm et al. Herwig 7.0/Herwig++ 3.0 release note. *Eur. Phys. J. C*, 76(4):196, 2016.
  - [5] K. Arnold et al. VBFNLO: A Parton level Monte Carlo for processes with electroweak bosons. *Comput. Phys. Commun.*, 180:1661–1670, 2009.
  - [6] J. Baglio et al. VBFNLO: A Parton Level Monte Carlo for Processes with Electroweak Bosons – Manual for Version 2.7.0. 7 2011.
  - [7] J. Baglio et al. Release Note - VBFNLO 2.7.0. 4 2014.
  - [8] Julien Baglio, Francisco Campanario, Tinghua Chen, Heiko Dietrich-Siebert, Terrance Figy, Matthias Kerner, Michael Kubocz, Duc Ninh Le, Maximilian Löschner, Simon Plätzer, et al. Release note: Vbfnlo 3.0. *The European Physical Journal C*, 84(10):1003, 2024.
  - [9] Albert M Sirunyan et al. Observation of the Production of Three Massive Gauge Bosons at  $\sqrt{s} = 13$  TeV. *Phys. Rev. Lett.*, 125(15):151802, 2020.
  - [10] Georges Aad et al. Evidence of  $W\gamma\gamma$  Production in  $pp$  Collisions at  $\sqrt{s} = 8$  TeV and Limits on Anomalous Quartic Gauge Couplings with the ATLAS Detector. *Phys. Rev. Lett.*, 115(3):031802, 2015.
  - [11] Morad Aaboud et al. Search for triboson  $W^\pm W^\pm W^\mp$  production in  $pp$  collisions at  $\sqrt{s} = 8$  TeV with the ATLAS detector. *Eur. Phys. J. C*, 77(3):141, 2017.
  - [12] M. Aaboud et al. Study of  $WW\gamma$  and  $WZ\gamma$  production in  $pp$  collisions at  $\sqrt{s} = 8$  TeV and search for anomalous quartic gauge couplings with the ATLAS experiment. *Eur. Phys. J. C*, 77(9):646, 2017.
  - [13] Robert V Harlander, Sven Yannick Klein, and Maximilian Lipp. Feyngame. *Computer Physics Communica-*

- tions, 256:107465, 2020.
- [14] Robert Harlander, Sven Yannick Klein, and Magnus Schaaf. Feyngame-2.1—feynman diagrams made easy. *arXiv preprint arXiv:2401.12778*, 2024.
- [15] Simon Platzer and Stefan Gieseke. Dipole Showers and Automated NLO Matching in Herwig++. *Eur. Phys. J. C*, 72:2187, 2012.
- [16] S. Catani and M. H. Seymour. A General algorithm for calculating jet cross-sections in NLO QCD. *Nucl. Phys. B*, 485:291–419, 1997. [Erratum: Nucl.Phys.B 510, 503–504 (1998)].
- [17] T. Binoth et al. A Proposal for a Standard Interface between Monte Carlo Tools and One-Loop Programs. *Comput. Phys. Commun.*, 181:1612–1622, 2010.
- [18] S. Alioli et al. Update of the Binoth Les Houches Accord for a standard interface between Monte Carlo tools and one-loop programs. *Comput. Phys. Commun.*, 185:560–571, 2014.
- [19] Michael Rauch and Simon Plätzer. Parton Shower Matching Systematics in Vector-Boson-Fusion WW Production. *Eur. Phys. J. C*, 77(5):293, 2017.
- [20] G. Bozzi, F. Campanario, M. Rauch, H. Rzehak, and D. Zeppenfeld. NLO QCD corrections to  $W^\pm Z\gamma$  production with leptonic decays. *Phys. Lett. B*, 696:380–385, 2011.